# Serveur Académique Lausannois SERVAL serval.unil.ch

# Author Manuscript
## Faculty of Biology and Medicine Publication

This paper has been peer-reviewed but dos not include the final publisher proof-corrections or journal pagination.

Published in final edited form as:

serval
serveur académique lausannois

UNIL | Université de Lausanne
Faculté de biologie
et de médecine

# VESSEL CENTERLINE TRACKING AND BOUNDARY SEGMENTATION IN CORONARY MRA WITH MINIMAL MANUAL INTERACTION

**Sahar Soleimanifard**[1], **Michael Schär**[2,4], **Allison G. Hays**[2,3], **Robert G. Weiss**[2,3], **Matthias Stuber**[2,5], and **Jerry L. Prince**[1,2]

[1]Department of Electrical and Computer Engineering, Johns Hopkins University, Baltimore, MD, USA [2]Department of Radiology, Johns Hopkins University, Baltimore, MD, USA [3]Division of Cardiology, Department of Medicine, Johns Hopkins University, Baltimore, MD, USA [4]Philips Healthcare, Cleveland, OH, USA [5]Department of Radiology, University of Lausanne, Lausanne, Switzerland

## Abstract

Magnetic resonance angiography (MRA) provides a noninvasive means to detect the presence, location and severity of atherosclerosis throughout the vascular system. In such studies, and especially those in the coronary arteries, the vessel luminal area is typically measured at multiple cross-sectional locations along the course of the artery. The advent of fast volumetric imaging techniques covering proximal to mid segments of coronary arteries necessitates automatic analysis tools requiring minimal manual interactions to robustly measure cross-sectional area along the three-dimensional track of the arteries in under-sampled and non-isotropic datasets. In this work, we present a modular approach based on level set methods to track the vessel centerline, segment the vessel boundaries, and measure transversal area using two user-selected endpoints in each coronary of interest. Arterial area and vessel length are measured using our method and compared to the standard Soap-Bubble reformatting and analysis tool in *in-vivo* non-contrast enhanced coronary MRA images.

### Index Terms

3D Centerline Tracking; 3D Segmentation; Level Set Methods; Non-contrast enhanced Magnetic Resonance Angiography; Coronary Arteries

## 1. INTRODUCTION

Coronary atherosclerotic disease is a major cause of morbidity and mortality characterized by spatially heterogeneous plaque formation that can narrow or occlude the coronary artery lumen in severe disease. Coronary magnetic resonance angiography offers a powerful means to non-invasively identify significant atherosclerotic disease that narrows the coronary artery luminal area [1]. Studies to date measure the two-dimensional (2D) cross-sectional luminal area at a few segments in each artery [1], in part due to limitations in three-dimensional (3D) fast imaging techniques and in part due to extensive manual interactions. Introduction of rapid 3D volumetric techniques for imaging coronary arteries in higher field systems necessitates automatic analysis tools with minimal interactions for robust and reproducible quantification of luminal area along the 3D arterial pathway in the presence of noise, partial volume effects, and motion artifacts.

Coronary arteries usually exhibit high variability in size and curvature and are often surrounded by other structures which make segmentation a challenging task. There have been many algorithms proposed for 3D segmentation of curvilinear structures in medical imaging with general or acquisition-dependent considerations and mainly focused on contrast-enhanced acquisitions [2, 3]. Vessels are usually represented (1) by parametric cylinder-like tubes or (2) by a general deformable surface to capture tree-like structures (the reader may refer to [4] for a comprehensive overview). While the first approach is not flexible enough to handle branching, the latter has many degrees of freedom and can be modified per application. Parametric and geometric deformable models, incorporating image features, region statistics, and textural information, are widely used and have proven to be efficient in extraction of tubular structures [2]. Geometric deformable models, often implemented via level set methods [5], possess the intrinsic advantage of handling topological changes and do not suffer from parameterization problems inherent to parametric models. However, these models are sensitive to initialization and propagation forces and are computationally expensive.

In this work, we propose a modular approach for segmentation of coronary artery boundaries based on geometric deformable models and optimized energy forces. We discuss the motivation behind our optimization scheme and incorporation of prior shape information of tubular structures using second-order image information in addition to traditional edge-based features, which may not be well defined in under-sampled and non-isotropic datasets. We utilize the fast marching and level set methods [5] to robustly segment the vessel boundary and measure cross-sectional area at a sub-voxel resolution using two manually identified endpoints on each coronary. We characterized the efficacy of our proposed technique in comparison with Soap-Bubble, the standard coronary analysis tool [6], in non-contrast enhanced *in-vivo* MRA images (Fig. 1A). Segmentation in such images is especially challenging due to lack of extraneous contrast between coronary blood pool and the surrounding tissue.

## 2. METHODS

### 2.1. Tubular structures

The eigenvalue decomposition of the Hessian matrix of a 3D image extracts the local second order information, which varies among different structures (Table 1). The eigen decomposition can be performed by convolving the image with the second partial derivatives of an isotropic Gaussian kernel. This property of eigenvalues has been previously adopted to construct vessel-enhancement filters [7], which we employ in our proposed vessel tracking framework to artificially increase the contrast between vessel-like structures and other structures (Fig. 1B). In addition to eigenvalues, we use the information of eigenvectors (principal directions of local change) in our segmentation scheme. In tubular structures, the eigenvector $\hat{e}_1$ corresponding to the smallest eigenvalue $\lambda_1$ points in the longitudinal direction of the vessel (Fig. 1C), which has the smallest curvature and the normal plane to this direction (i.e., eigenvectors corresponding to $\lambda_2$ and $\lambda_3$) forms the cross-sectional plane to the vessel.

### 2.2. Vessel centerline tracking

On each coronary of interest, the user identifies two endpoints as shown in Fig. 1A (the only manual interaction required). The automatic 3D path tracking between the two fixed endpoints can be mapped into a minimal path problem. Defining a cost function, the minimal path becomes the path for which the integral of costs is minimum. This minimal cost satisfies the Eikonal equation and can be reformulated into a boundary value formulation [8]:

$$F|\nabla U|=1 \quad (1)$$

where $U$ is the minimal energy integrated along a path between two points and $F$ is a potential map that takes larger values near desired features. The well-known fast marching algorithm [5] can numerically solve this equation and yield the minimum path [8].

In this work, we use the multi-scale vessel-enhancement filter [7] and an edge function to construct this potential map:

$$F=V\frac{1}{1+\left\|\nabla(G*I)\right\|^2} \quad (2)$$

$V$ is the vessel-enhanced image (eighteen linearly increasing scales, σ=0.4–4), $G$ is a Gaussian kernel (σ=0.5), and $I$ is the image intensity function. Using the vessel-enhanced image as the potential map, the tracked centerline falls inside the vessel. However, in regions of constant $V$, it leads to the shortest Euclidean path. The reciprocal of the edge map creates smaller values close to edges and centers the tracked path in regions where $V$ is constant. Fig. 1E illustrates one example of a tracked centerline in an RCA using the vessel-enhanced image (Fig. 1B) and the edge map (Fig. 1D). The centerline, once tracked, is used to initialize the boundary segmentation.

## 2.3. Vessel boundary segmentation

Segmentation can be regarded as the evolution of a front, or interface, toward the boundaries of a structure. The geodesic active contour model [9] implemented via level set methods [5], implicitly defines this interface as the zero level set of a higher dimensional function. The classic formulation tracks the moving interface under forces depending on the intrinsic properties of the higher dimensional function and the external constraints:

$$\frac{\partial \varphi}{\partial t}+A \cdot \nabla\varphi+F|\nabla\varphi|=0 \quad (3)$$

where $\varphi$ is the level set function (LSF) (usually initialized via a signed distance function), with zero level set representing the implicit surface. A scalar speed function $F$, and a 3D vector field $A$, together act as inflationary and stopping forces.

For the task of segmenting the coronary artery boundaries, we construct a geodesic active contour model in the following way:

$$\frac{\partial \varphi}{\partial t}+gH\frac{\nabla(G*I)}{|\nabla(G*I)|} \cdot \nabla\varphi+g(\nu-\varepsilon\kappa)|\nabla\varphi|+R(\nabla\varphi)=0 \quad (4)$$

where Hessian matrix $H$ and edge map of the image intensity $I$, form the vector field $A$ [10]. The constant unidirectional force $\nu$ and mean curvature $\kappa$ of the LSF ($\nabla\cdot (\nabla \varphi / |\nabla \varphi|)$) with a weighting factor $\varepsilon$ form the speed function $F$. The vector field and speed function evolve the zero level set from an initial state (vessel centerline in our implementation) towards the vessel boundaries. Traditionally, an edge-based strictly decreasing function $g$ ($g(r) \to 0$ as $r \to \infty$) using image gradients is added to stop the zero level set on object boundaries and balance the inflationary forces. However, the use of image information alone often leads to poor segmentation results in the presence of noise and outliers. A combination of the edge information and vessel-enhanced image has been previously used to address this problem in contrast-enhanced MRA [11], however, this implementation results in thin vessels due to

lack of soft tissue contrast in our images (Fig. 4). To address this problem, we construct the stopping term $g$ by adopting the vascularity-oriented information from the eigen decomposition of the Hessian matrix. The eigenvector $\hat{e}_1$ corresponding to $\lambda_1$ creates a 3D vector field where the vectors inside the vessel and near the centerline point to the longitudinal direction of the vessel (Fig. 1C). The vectors deviate from this direction as they become farther from the centerline and the penalty on this deviation forms the basis for our proposed stopping term $g$. First, noise and outliers are removed from the vector field using similarity to a pattern in the neighborhood of each vector (detailed description not included due to space limitations. The reader may refer to [12] for more information). Then the penalty function is defined at every voxel in the volume as the angle between the eigenvector at that voxel and the eigenvector at the closest point on the vessel centerline:

$$P(\mathbf{x}) = \angle \left( \widehat{e_1}(\mathbf{x}), \widehat{e_1}(\mathbf{x}_{center}) \right) \quad (5)$$

where $\mathbf{x} = (x, y, z)$ is a voxel in 3D space and $\mathbf{x}_{center}$ is the closest point to $\mathbf{x}$ on the vessel centerline. The stopping term $g$ is then defined as:

$$g = \frac{1}{1 + \left\| \nabla(G * P) \right\|^2} \quad (6)$$

where $G$ is the Gaussian kernel ($\sigma = 0.3$) and $P$ is the penalty function. We also limit the evolution of LSF to a portion of volume with $P(\mathbf{x}) < \theta_0$ to further reduce the computational time. For our application, $\nu = 1$, $\varepsilon = 1$, and $\theta_0 = \pi/4$ worked well in practice.

In conventional level set methods, the LSF develops irregularities during evolution, which leads to instability. To overcome this problem, a reinitialization is performed periodically by stopping the evolution and reshaping the LSF as a signed distance function, which results in computational cost. To eliminate the need for reinitialization, we use a previously proposed additional term $R(\nabla \varphi)$ in the level set formulation [13], which is a double-well function with two minimums. This function is aimed to maintain the signed distance property $|\nabla \varphi| = 1$ only in a vicinity of the zero level set, while keeping the LSF as a constant, with $|\nabla \varphi| = 0$, at locations far away from the zero level set (refer to [13] for detailed description). Fig. 2A illustrates the segmented boundary for the artery shown in Fig. 1.

## 2.4. Cross-sectional plane identification

Once the vessel boundary is segmented, orthogonal planes to the vessel centerline must be identified at every point on the coronary of interest to measure lumen area. For this purpose, the eigenvectors of the Hessian matrix are reselected at every point inside the segmented boundary. The eigenvectors corresponding to $\lambda_2$ and $\lambda_3$ form the orthogonal plane to the longitudinal direction of the vessel (Fig. 2B). The intersection of this plane and the segmented boundary yields the arterial area with a sub-voxel resolution due to level set implementation.

## 2.5. *In-vivo* experiments

Volume targeted 3D navigator-gated free breathing MRA [14] images covering proximal to mid segments of coronary arteries were acquired on a whole body 3.0T scanner (Achieva, Philips Healthcare, Best, The Netherlands) in ten healthy adult volunteers (RCA: n = 6, LAD: n = 4). Scan parameters were the following: repetition time = 4.1ms, echo time = 1.5ms, flip angle = 20°, radio frequency excitations per k-space segment = 25, field of view = 300×300×32mm$^3$, acquired voxel size = 1.0×1.0×2.0mm$^3$, reconstructed voxel size = 0.8×0.8×1.0mm$^3$, scan time ~ 5min. Sinc interpolation was used to convert the anisotropic voxels to isotropic voxels on a separate workstation.

### 2.6. Analysis and validation

The Soap-Bubble reformatting and analysis tool [6] was used to validate our vessel centerline tracking and area measurements. Using Soap-Bubble tool, the 3D pathway of each coronary artery was manually identified and used to perform multi-planar reformatting. Cross-sectional diameters and area (assuming a circular cross-section) along this 3D pathway were calculated from the edge profile of the reformatted image using the Deriche algorithm. The two endpoints of the user-selected points were reselected and used as seed points for automatic vessel centerline tracking and boundary segmentation using our proposed framework. To quantify the method's performance in comparison to Soap-Bubble, linear regression and Bland-Altman plots were generated comparing vessel length measurements and area measurements averaged over 9mm segments. The rationale for using 9mm segments was that 9mm is the slice thickness of 2D cross-sectional scans routinely used in our coronary studies [1]. In addition, precision was defined as the standard deviation of area within each 9mm-segment to quantify the error of measurements. Two-sided paired Student $t$ test was used to compare precision of measurements in Soap-Bubble tool and the proposed method.

## 3. RESULTS AND DISCUSSION

Vessel length was measured in ten datasets using the new centerline tracking method and compared to results from Soap-Bubble tool using manual identification. Fig. 3 illustrates the scatter plot and the Bland-Altman plot of the two measurements. Linear regression exhibits a strong correlation (R=0.997) between the two techniques. The mean difference of the two measurements was 0.083mm (confidence interval (CI): (−0.628, 0.792), p = NS).

We compared the performance of our proposed propagation forces in the level set implementation with previous published methodology. Fig. 4 compares measured cross-sectional areas in an example RCA from Soap-Bubble tool and (1) $g$ function constructed using image intensities and $\nu = 0$ [10], (2) $g$ function constructed using vessel-enhanced image $V$ and $A = 0$ [11], and (3) our implementation. Our method exhibits strong agreement with Soap-Bubble results while not showing large variation of measured areas within short segments of the artery.

To quantitatively assess the performance of the boundary segmentation algorithm, cross-sectional areas were measured along each coronary artery (n=10) and averaged over 9mm-segments (n=63). The scatter plot of the area pairs measured using our proposed method and Soap-Bubble tool is shown in Fig. 5A. R=0.923 confirms strong correlation between results of the two techniques. Given the interpolated voxel dimensions ($0.8{\times}0.8{\times}0.8mm^3$), mean area difference of $−0.153mm^2$ (CI: (−0.374, 0.068), p = NS) between the cross-sectional area measures (Fig. 5B) demonstrates close agreement between the two techniques and accuracy of our proposed segmentation framework.

In addition, the average precision of area measures using our proposed method was found to be significantly higher compared to that of the Soap-Bubble tool ($0.57{\pm}0.27mm^2$ vs. $0.83{\pm}0.46mm^2$, p<0.0001).

## 4. CONCLUSION AND FUTURE WORK

We proposed automatic vessel centerline tracking and boundary segmentation algorithms to robustly measure the area of major coronary arteries. Results from our method are in strong agreement with Soap Bubble tool while requiring smaller manual interactions. The advantage of our proposed framework in comparison with methods that directly segment the boundary is that the tracked centerline can also be used for maximum intensity projection,

often used for visualization of coronary arteries. The performance of the proposed framework was investigated in non-contrast enhanced MRA images. The proposed methodology, however, can be also applied to contrast-enhanced acquisitions.

In our future work, this framework will be validated and compared with a gold standard (manual delineation) and its performance will be tested in presence of bifurcations and stenosis in patients with coronary artery disease.

## Acknowledgments

## References

1. Hays AG, Hirsch GA, Kelle S, Gerstenblith G, Weiss RG, Stuber M. Noninvasive Visualization of Coronary Artery Endothelial Function in Healthy Subjects and in Patients With Coronary Artery Disease. Journal of the American College of Cardiology. 2010; 56:1657–1665. [PubMed: 21050976]

2. Lesage D, Angelini ED, Bloch I, Funka-Lea G. A review of 3D vessel lumen segmentation techniques: Models, features and extraction schemes. Medical Image Analysis. 2009; 13:819–845. [PubMed: 19818675]

3. Schaap M, Metz CT, van Walsum T, et al. Standardized evaluation methodology and reference database for evaluating coronary artery centerline extraction algorithms. Medical Image Analysis. 2009; 13:701–714. [PubMed: 19632885]

4. Kirbas C, Quek F. A review of vessel extraction techniques and algorithms. ACM Comput Surv. 2004; 36:81–121.

5. Sethian, JA. Level Set Methods and Fast Marching Methods. Cambridge University Press; 1999.

6. Etienne A, Botnar RM, van Muiswinkel AMC, Boesiger P, Manning WJ, Stuber M. "Soap-Bubble" visualization and quantitative analysis of 3D coronary magnetic resonance angiograms. Magnetic Resonance in Medicine. 2002; 48:658–666. [PubMed: 12353283]

7. Frangi A, Niessen W, Vincken K, Viergever M. Multiscale vessel enhancement filtering. Medical Image Computing and Computer-Assisted Intervention. 1998; 1496:130–137.

8. Cohen LD, Kimmel R. Global Minimum for Active Contour Models: A Minimal Path Approach. International Journal of Computer Vision. 1997; 24:57–78.

9. Caselles V, Kimmel R, Sapiro G. Geodesic Active Contours. International Journal of Computer Vision. 1997; 22:61–79.

10. Lorigo LM, Faugeras OD, Grimson WEL, Keriven R, Kikinis R, Nabavi A, Westin CF. CURVES: Curve evolution for vessel segmentation. Medical Image Analysis. 2001; 5:195–206. [PubMed: 11524226]

11. van Bemmel CM, Spreeuwers LJ, Viergever MA, Niessen WJ. Level-set-based artery-vein separation in blood pool agent CE-MR angiograms. Medical Imaging, IEEE Transactions on. 2003; 22:1224–1234.

12. Soleimanifard S, Abd-Elmoniem KZ, Murano EZ, Abraham MR, Abraham TP, Prince JL. Three-dimensional Principal Strain Patterns in Acute Myocardial Infarction. Proceedings of ISMRM. 2011

13. Chunming L, Chenyang X, Changfeng G, Fox MD. Distance Regularized Level Set Evolution and Its Application to Image Segmentation. Image Processing, IEEE Transactions on. 2010; 19:3243–3254.

14. Stuber M, Botnar RM, Danias PG, Sodickson DK, Kissinger KV, Van Cauteren M, De Becker J, Manning WJ. Double-oblique free-breathing high resolution three-dimensional coronary magnetic resonance angiography. Journal of the American College of Cardiology. 1999; 34:524–531. [PubMed: 10440168]
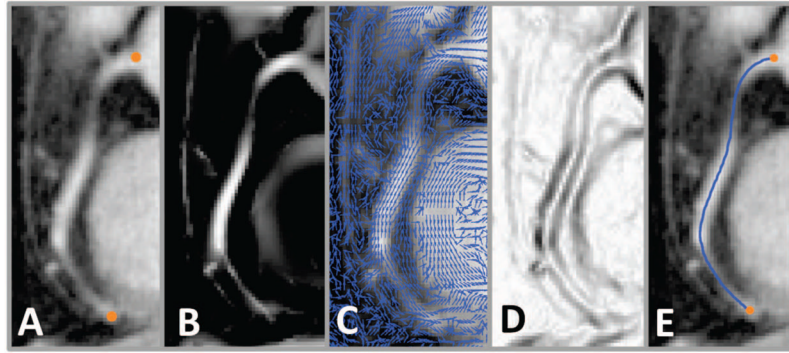
**Figure 1. Example of a right coronary artery**
(**A**) Middle slice of the 3D volume selected for visualization, (**B**) Vessel-enhanced image, (**C**) Eigenvectors corresponding to $\lambda_1$ of Hessian matrix, (**D**) Edge map, and (**E**) Two endpoints (orange circles) manually identified to track the vessel centerline (blue line).
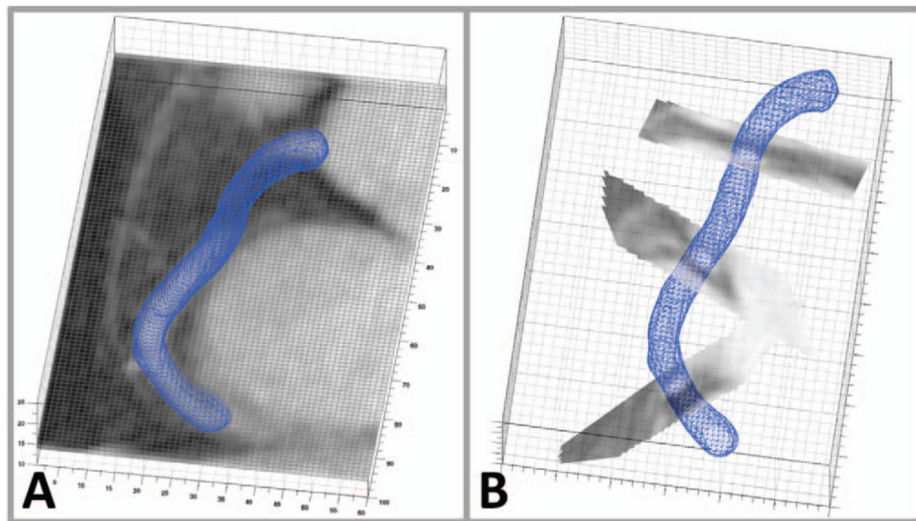
**Figure 2.**
**(A)** Vessel boundary segmented using the tracked vessel centerline as the initial boundary (Fig. 1E), **(B)** Cross-sectional planes to the vessel identified using eigenvectors of Hessian matrix (Fig. 1C).
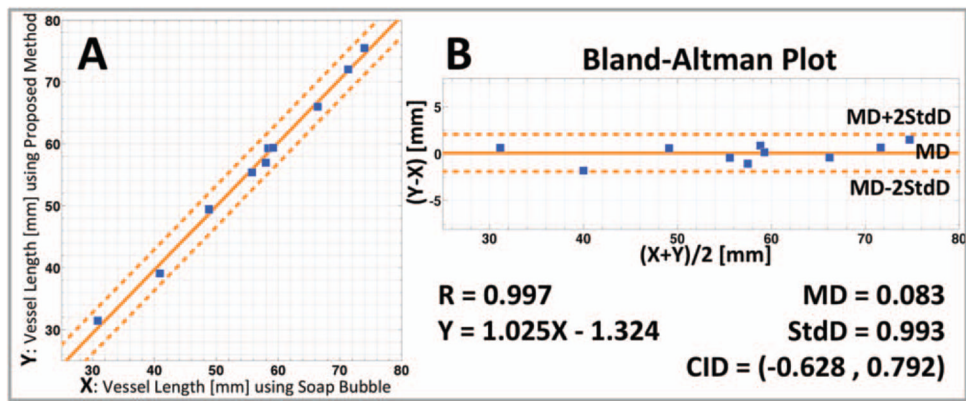
**Figure 3. Vessel length measurements in 10 normal volunteers**
**(A)** Scatter plot show strong correlation (R = 0.997) for measurements with Soap-Bubble tool (X) and the proposed method (Y). Dotted lines represent confidence interval (CI) lines. **(B)** Bland-Altman plot. MD: mean difference. StdD: standard deviation of difference. CID: CI of difference.
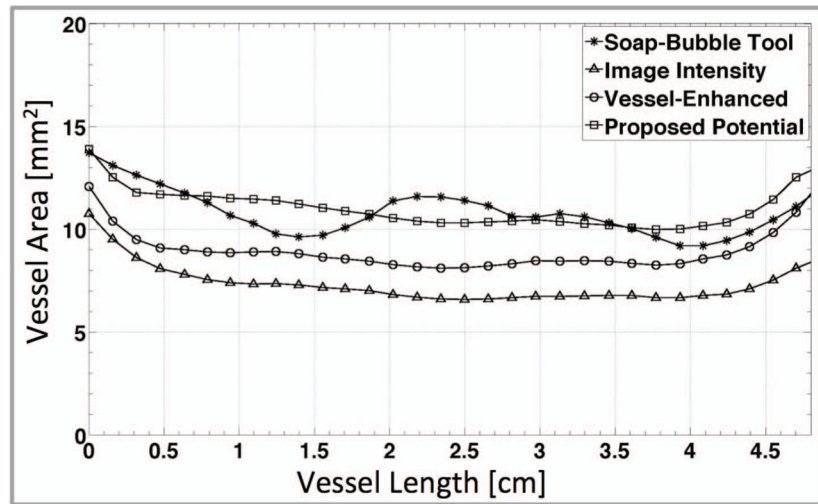
**Figure 4. Vessel cross-sectional areas in an example RCA**
Proximal arterial area (4.5cm from ostium) is measured using Soap-Bubble tool and three implementations of level set methods.
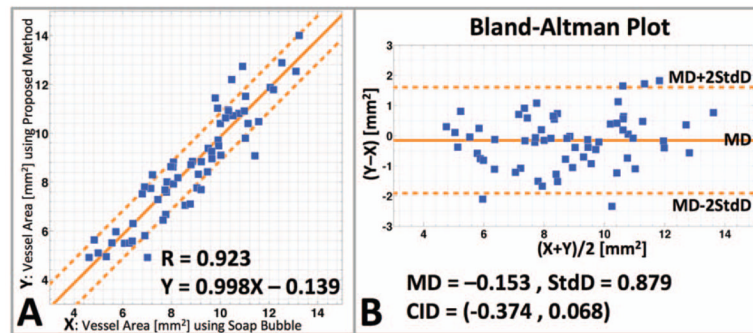
**Figure 5. Vessel cross-sectional area averaged in 9mm-long segments (n=63)**
(**A**) Scatter plot show strong correlation (R=0.923) for measurements with Soap-Bubble tool (X) and the proposed implementation (Y). Dotted lines represent confidence interval (CI) lines. (**B**) Bland-Altman plot. MD: mean difference. StdD: standard deviation of difference. CID: CI of difference.

**Table 1**

Pattern profiles in 3D images, depending on the value of the eigenvalues of the Hessian matrix ($|\lambda_1|$ $|\lambda_2|$ $|\lambda_3|$).

| Image Patterns | $\lambda_1$ | $\lambda_2$ | $\lambda_3$ |
|---|---|---|---|
| Tubular Structures | Low | High | High |
| Blob-like Structures | High | High | High |
| Plate-like Structures | Low | Low | High |
| Noise | Low | Low | Low |